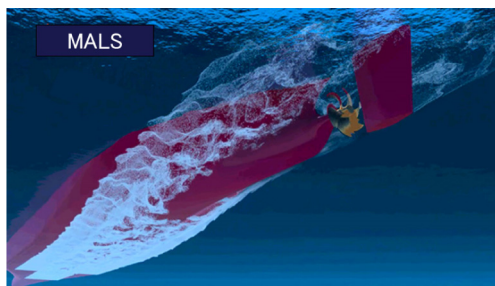


Application of Simulation Technology to Mitsubishi Air Lubrication System



CHIHARU KAWAKITA*¹ SHINSUKE SATO*²

TAKAHIRO OKIMOTO*²

For the development and design of the Mitsubishi Air Lubrication System (hereafter MALS), which targets energy saving in ships, the utilization of simulation technology is essential. This paper describes the key technology for the development of MALS, which is CFD-based prediction technology for air bubble distribution around a hull, and also presents the frictional drag reduction effect. It also presents a prediction technology for the pressure fluctuation of a propeller that rotates in the bubbly flow, as well as a related technology for the prediction of gas-liquid separation in a sea chest that is an engine cooling water suction port. The prediction accuracy of these technologies has been verified and enhanced through verification in actual ship tests and model tests, and therefore they are used as effective development and design tools. Also in the future, MHI will continuously obtain data from the measurement results of actual ships and utilize it for the performance enhancement of MALS.

1. Introduction

The development of energy-saving ships is greatly anticipated by the shipping industry as a countermeasure against the surging prices of resources including oil, and environmental issues such as CO₂ emission regulations for international shipping operations. The air lubrication method, which reduces frictional drag by mixing air bubbles of millimeter order into the flow around the hull, has attracted attention because it can be expected to result in an especially significant energy-saving effect among other energy-saving technologies. In April 2010, MHI completed Yamatai, a module carrier ordered by NYK-Hinode Line, Ltd., which was the world's first newly built ship equipped with the Mitsubishi Air Lubrication System (MALS) advanced air lubrication method.

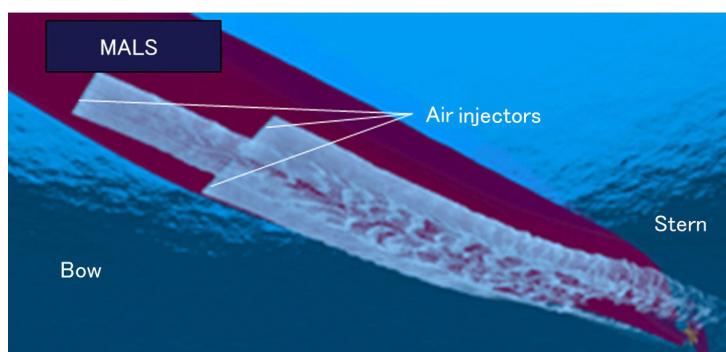


Figure 1 Image of ship equipped with MALS

The bottom of the ship is covered by air bubbles released from the air injectors.

Figure 1 shows a conceptual image of a ship equipped with MALS. The ship achieved an energy-saving effect of more than 10% attributable to MALS during actual ship tests in a sea trial⁽¹⁾. In December 2010, MHI completed Yamato, Yamatai's sister ship, which was also equipped with MALS. Using Yamato, the energy-saving effect was verified in a sea trial, the flow of air bubbles around the ship bottom was observed with a towed underwater vehicle as shown in **Figure 2**, and the local frictional drag was measured by shear stress sensors installed on the bottom

*1 Chief Staff Manager, Nagasaki Research & Development Center, Technology & Innovation Headquarters

*2 Nagasaki Research & Development Center, Technology & Innovation Headquarters

of the ship. As a result, actual ship data valuable for the enhancement of the frictional drag reduction effect of MALS were acquired. As four years have elapsed since the module carrier went into service, MALS is still working without any major failures. MHI is now aiming at expanding MALS to ferries, bulk carriers, and large passenger ships⁽²⁾.

This paper describes the main simulation technology utilized for the design of MALS. First, the flowchart of the energy-saving effect prediction attributable to MALS will be presented, and then the key technology for the estimation of the energy-saving effect resulting from MALS, which is CFD-based prediction technology for air bubble distribution around a hull, will be explained together with the frictional drag reduction effect. MHI is working hard on the enhancement of the prediction accuracy of this technology by obtaining data acquired in actual ship tests and model tests. In addition, a prediction technology for the pressure fluctuation of a propeller that rotates in the bubbly flow, as well as a prediction technology for gas-liquid separation in a sea chest that is an engine cooling water suction port, will be introduced as related technologies.

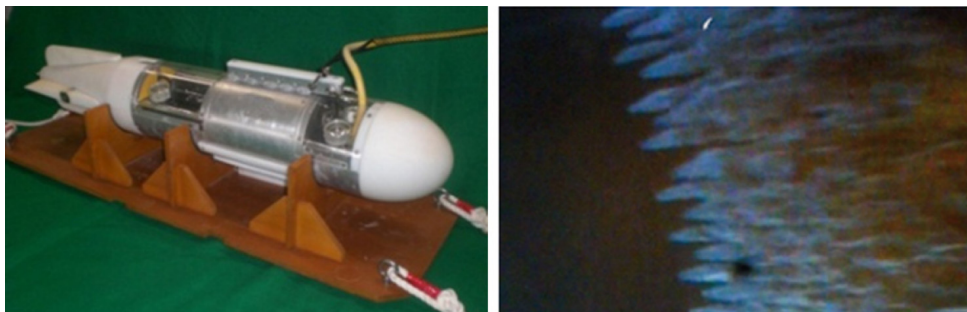


Figure 2 Towed underwater vehicle and air bubble flow released from air injector
The flow of air bubbles around the ship bottom was observed with a towed underwater vehicle containing a camera (left photograph) to verify that the air bubbles were released uniformly from the air injector (right photograph) and that air bubbles did not leak to the side of the ship.

2. Flowchart of energy-saving effect prediction attributable to MALS

Although the propulsive power of a typical ship is estimated from the results of a tank test using a model ship, it is difficult to estimate the propulsive power of a ship equipped with MALS in this manner. This is because it is necessary to facilitate the flow of air bubbles of micrometer order around the model ship hull (compared with air bubbles of millimeter order around an actual ship) according to the model size, which is difficult to do by simple blowing air from the model ship. Therefore the tank test, for which there is no choice but to use air bubbles larger than the scale ratio of the model, results in the underestimation of the frictional drag reduction effect and air bubble distribution around the propeller. For this reason, it is necessary and important for the estimation of the energy-saving effect of a ship equipped with MALS to use a prediction technology that combines a tank test and a CFD-based prediction method of the frictional drag reduction effect.

Figure 3 shows the assumed flow of the energy-saving effect attributable to MALS. First, the air injector location and the amount of air blow-off volume are set, and then the air bubble distribution (void fraction distribution) around the hull and the propeller is estimated using the results of CFD-based simulation of the air bubble flow around the hull. Next, data of the void fraction distribution in the vicinity of the hull surface is input and the simulation of the reduction in frictional drag is performed using MHI's proprietary frictional drag reduction model. With reference to the void fraction distribution at the location of the propeller acquired from the simulation of the air bubble flow around the hull, the efficiency of the propeller in the bubbly flow and the change in the propeller pressure fluctuation that is necessary for the prediction of hull vibration are estimated using a combination of experiments and simulation. Finally, the net energy-saving effect is obtained by estimating the power needed for air blow and subtracting it from the energy-saving effect of the reduction in frictional drag. In addition, the amount of air bubbles taken into the sea chest is estimated based on the void fraction distribution around the hull to determine the shape and internal structure that can perform gas-liquid separation successfully, based on the gas-liquid simulation in the sea chest.

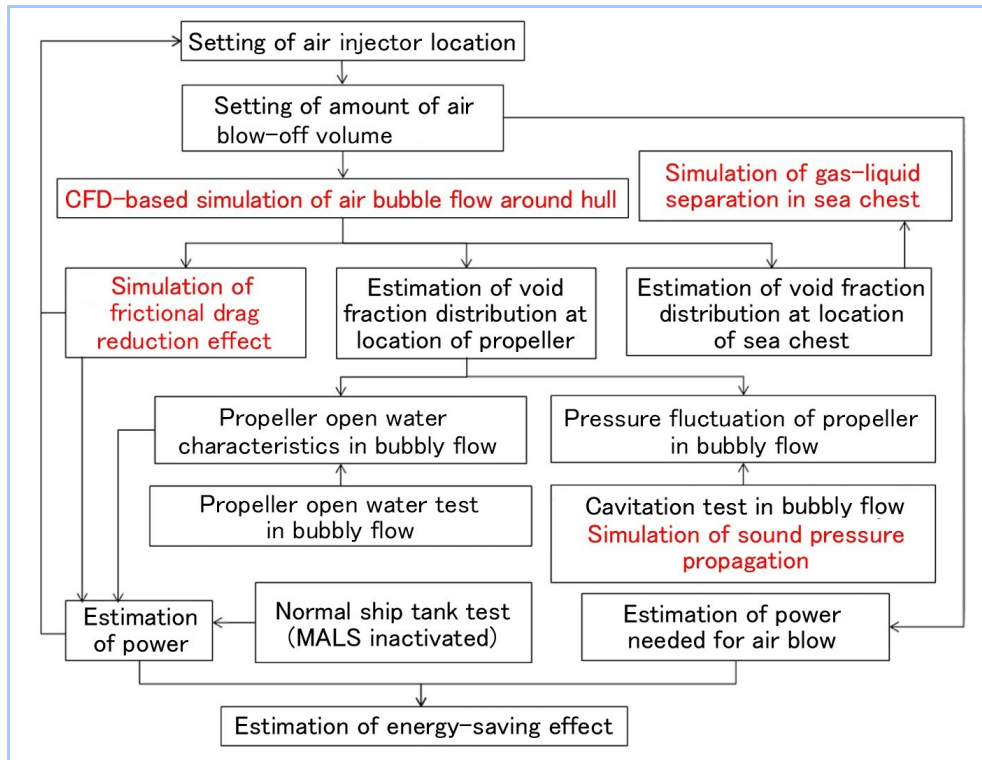


Figure 3 Flowchart of energy-saving effect prediction attributable to MALS

3. CFD-based prediction technology for air bubble distribution around a hull and frictional drag reduction effect

The air bubble flow model used for CFD-based simulation of the air bubble flow around the hull consists of a continuous expression of the mixed phase, a momentum equation of the mixed phase, a conservation equation of the air bubble void fraction and a translation motion equation of air bubbles being the governing equation. The estimation of the frictional drag reduction effect uses MHI's proprietary frictional drag reduction model based on the corresponding air film thickness acquired by integrating the air bubble distribution in a boundary layer around the hull in the direction vertical to the solid wall. This frictional drag reduction model is the application of a wall function against a rough surface. In this model, the frictional drag increases on a rough surface and is reduced through the use of an air lubrication method⁽³⁾.

3.1 Calculation flow

Actual calculation proceeds in the order of single-phase flow calculation without flowing air bubbles, one-way calculation, two-way calculation, and three-way calculation. A summary of each calculation is as follows:

(1) One-way calculation

Bubble flow calculation is performed using the density, viscosity and normal eddy viscosity coefficient of water. The air bubbles are solved as a passive scalar. The flow of the liquid phase influences the gas phase, but the flow of the gas phase does not influence the liquid phase. This calculation is known as a one-way calculation, and can obtain the air bubble distribution.

(2) Two-way calculation

The result of the one-way calculation is read. The calculation is performed with the density and viscosity changing depending on the void fraction. The flow of the gas phase influences the liquid phase, and therefore this calculation is known as a two-way calculation. The hull resistance changes based on the influence of the changing density and viscosity, but although both the frictional drag and the pressure resistance change, there is little frictional drag reduction effect because the influence of turbulence modulation caused by the air bubbles is not included. The void fraction distribution changes slightly due to the influence of density change.

(3) Three-way calculation

The result of the two-way calculation is read. The calculation is performed with the

aforementioned frictional drag reduction model activated. This calculation takes into consideration the reduction in the frictional drag and all flow changes caused thereby.

3.2 Calculation example

Calculation for the aforementioned module carrier with a length of 162 m, for which an actual ship test was conducted, was performed in order to verify the calculation accuracy. **Figure 4** shows the void fraction distributions around the hull and at the location of the propeller obtained through the simulation of the air bubble flow around the hull. The air bubbles flowed along the hull without leaking from the bottom of the hull to the side of the ship, and the air bubble flow observed in the actual ship test using a towed underwater vehicle was reproduced. The void fraction at the location of the propeller tended to increase in the vicinity of the bottom of the hull, and decrease with distance from the hull. **Figure 5** shows the calculation results of shearing force distribution on the bottom of the hull with MALS activated and inactivated. It is found that air bubbles covered a wide area of the bottom of the hull and the shearing force of the covered area decreased. **Figure 6** compares the actual ship test results and the calculation results of the local frictional drag reduction effect with the change in the amount of air blow-off volume. The tendency where the local frictional drag reduction effect increases more when the amount of air blow-off volume becomes larger could be evaluated by the calculation. It is found that the frictional drag reduction effect rises to as much as 60% when the amount of air blow-off volume is large. As the calculation accuracy also attained a quantitative result that was roughly consistent with the results of the actual ship test, this method is sufficiently applicable to the design of a ship equipped with an air lubrication system.

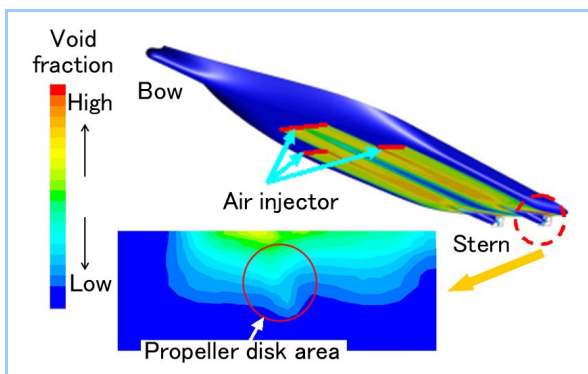


Figure 4 Void fraction distribution on hull surface and at the location of propeller

The upper figure shows the void fraction distribution of air bubbles flowing on the hull surface from the air injector to the stern. The lower figure shows a magnified view of the void fraction distribution at the location of the propeller on the port side.

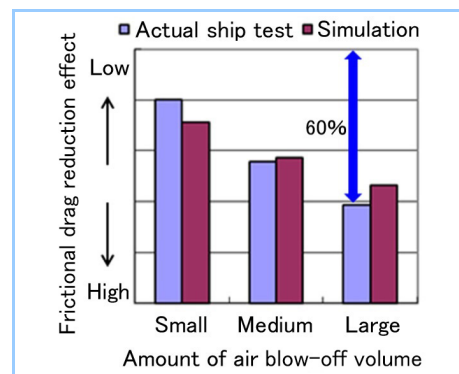


Figure 6 Comparison of local frictional drag reduction effect

The local frictional drag reduction effects based on the situation with MALS inactivated were compared. The lower the bar, the higher the frictional drag reduction effect.

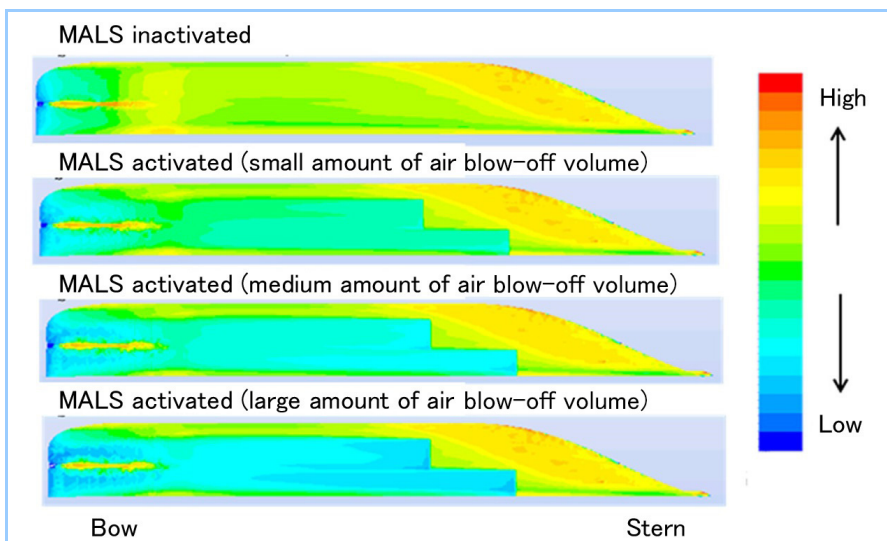


Figure 5 Prediction of frictional drag distribution on hull surface

The frictional drag distribution on the bottom of the hull on the port side viewed from below. The frictional drag decreased in a wide area of the bottom of the hull.

4. Prediction technology for increase/decrease in the pressure fluctuation of a propeller that rotates in the bubbly flow through simulation of sound pressure propagation

The air bubbles flowing around the hull are anticipated to flow into the propeller when a ship is equipped with MALS. Based on knowledge acquired from a tank test, it is known to lead to a decrease in efficiency of the propeller and increase/decrease in the pressure fluctuation of the propeller. An accumulation of air bubbles at the leading edge because of the pressure gradient contributes to the decrease in the efficiency of the propeller. On the other hand, it is becoming clear that the increase/decrease in the pressure fluctuation of the propeller is affected by the reflection, interference, and other phenomena of pressure waves at the air bubble layer between the propeller and the bottom of the hull.

In the examination of MALS, the increase/decrease of the pressure fluctuation of the propeller affected by the air bubbles is predicted through simulation technology for sound pressure propagation using the finite element method and the cavitation test in bubbly flow with the model propeller shown in **Figure 7**. The thickness of the air bubble layer and the void fraction distribution between the propeller and the bottom of the hull are set with reference to the void fraction distribution around the propeller obtained from the simulation of the air bubble flow around the hull. Then, the increase/decrease of the pressure fluctuation of the propeller corresponding to the propeller blade frequency is estimated using a calculation model that has a point pressure source simulating fluctuating cavitation on the propeller⁽⁴⁾.

For the study of a mechanism that increases the pressure fluctuation of a propeller, **Figure 8** shows the pressure fluctuation distributions for cases where an air bubble layer exists and where no air bubble layer (only water) exists, together with the air bubble layer thickness and the frequency which lead to the increase in the pressure fluctuation. In cases where the air bubble layer exists, the propeller pressure fluctuation at the bottom of the hull decreases due to the reflection of pressure waves at the boundary of the air bubble layer and the pressure damping effect in the air bubble layer. However, the standing wave (antinode-node-antinode) occurs in the direction of the air bubble layer thickness due to the interference of pressure waves in the air bubble layer and therefore the propeller pressure fluctuation at the bottom of the hull increases at the frequency where the standing wave occurs.

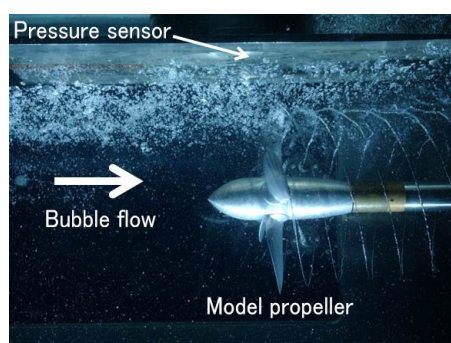


Figure 7 Cavitation test in bubbly flow

The propeller pressure fluctuation was measured by multiple pressure sensors embedded in the measuring plate immediately above the propeller. Air bubbles flowed from the air bubble release device installed on the upstream side.

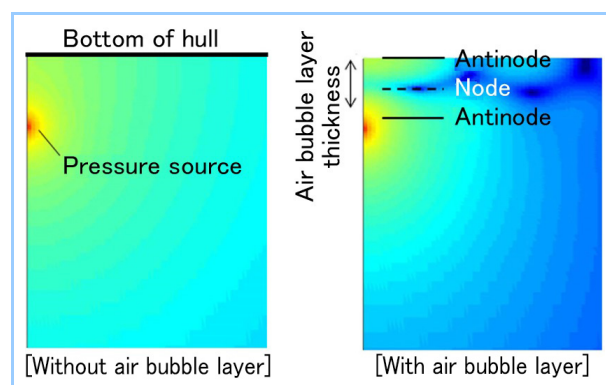


Figure 8 Change in pressure fluctuation distribution with and without air bubble layer

These are contour figures of the distributions of the pressure fluctuation propagating from the pressure source (red area) where the pressure fluctuation is high.

The propeller pressure fluctuation reduction effect was researched while maintaining a constant average void fraction in the air bubble layer and changing the air bubble layer thickness. Typically, the air bubble layer between the propeller and the bottom of the hull tends to have a higher void fraction when the layer is closer to the bottom of the hull. Therefore, with the average void fraction kept constant, the void fraction distribution in the air bubble layer has a higher void

fraction in the vicinity of the bottom of the hull when the air bubble layer thickness is thinner. **Figure 9** shows an example calculation result. This result represents no pressure fluctuation reduction effect in the lower frequency region. In the higher frequency region, however, the thinner the air bubble layer thickness becomes, the more the pressure fluctuation reduction effect increases. For this reason, the condition for reducing the propeller pressure fluctuation is regarded as the establishment of a thin air bubble layer with a high void fraction in the vicinity of the bottom of the hull. Assuming the development of a technology for controlling void fraction distribution at the location of the propeller, the disadvantageous risk of increasing propeller pressure fluctuation in a ship equipped with MALS might become the advantage of reducing the pressure fluctuation of a propeller. Such technologies include controlling the air bubble flow by providing new air bubble flow in the vicinity of the bottom of the hull from the upstream of the propeller or by collecting air bubbles flowing along the bottom of the hull in front of the propeller and releasing them again in the vicinity of the bottom of the hull on the upstream side of the propeller.

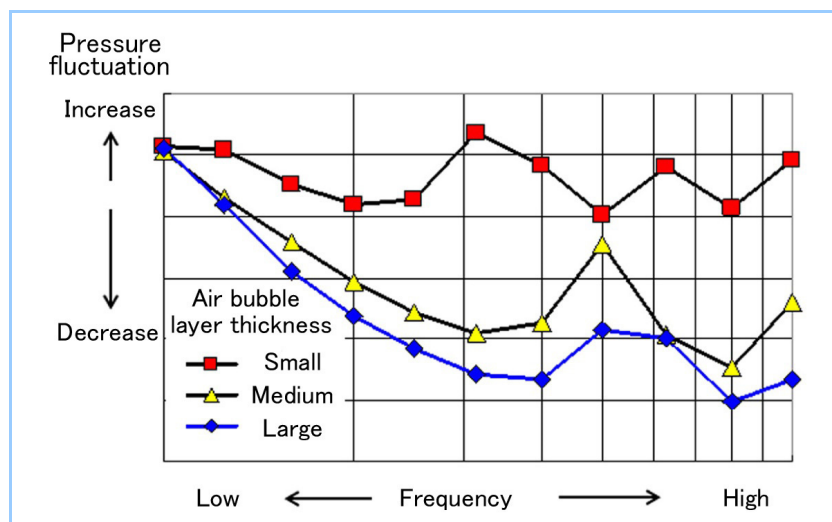


Figure 9 Change in pressure fluctuation of propeller depending on air bubble layer

This shows the change in the pressure fluctuation of the propeller corresponding to the change in the thickness of the air bubble layer between the propeller and the bottom of the hull and the change in the propeller blade frequency.

5. CFD-based prediction technology for gas-liquid separation in sea chest

A sea chest is a cooling water suction port placed on the stern bottom. A ship equipped with MALS runs the risk of a large amount of air bubbles flowing along the bottom of the hull being drawn into the sea chest and then taken into the pump, resulting in the deterioration of the pump performance and an adverse effect on engine cooling capacity. Therefore, the establishment of a shape and internal structure of a sea chest that can accurately separate gas from liquid is necessary. For this reason, MHI prepared a design standard for the determination of the shape and internal structure of a sea chest by utilizing the calculation results obtained from the simulation of gas-liquid separation in a sea chest using CFD shown in **Figure 10**.

For the effective confirmation of the simulation of gas-liquid separation in a sea chest, the estimation accuracy of the prediction technology for gas-liquid separation in a sea chest was verified through an experimental observation of the air bubble flow using a sea chest model. **Figure 11** gives example results of CFD calculation and experimental observation of the air bubble flow. The flow taken into the sea chest moved up along the partition plate. There occurred circulating flow at the top of the partition plate and air bubbles were separated from the liquid on a free-surface boundary between the gas phase and the liquid phase located on the circulating flow path. The flow pattern and the flow velocity of the calculation results were roughly consistent with those of the experimental results, and therefore this prediction technology was found to be effective for the examination of the gas-liquid separation structure in a sea chest.

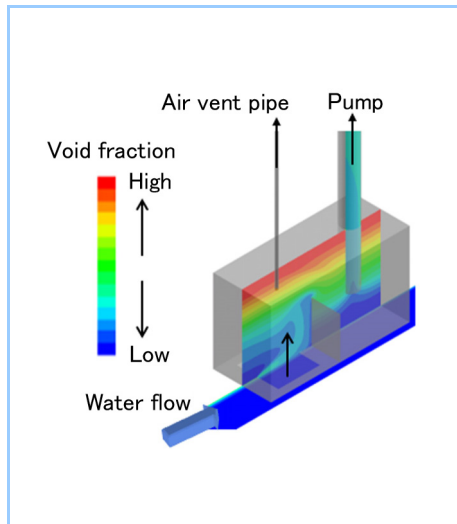


Figure 10 Simulation of gas-liquid separation in sea chest

Air bubbles flowing along the bottom of the hull are drawn into the sea chest, where gas-liquid separation occurs. This contour figure of the void fraction shows the gas-liquid separation.

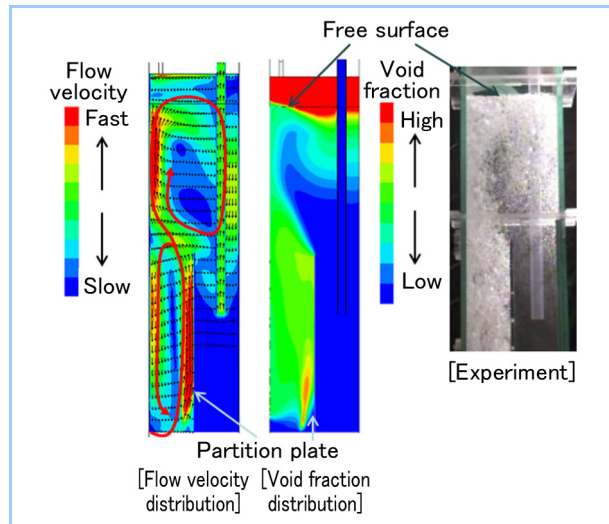


Figure 11 Flow velocity distribution and void fraction distribution in sea chest

This figure shows an experiment using a partial sea chest model and flow velocity distribution and void fraction distribution in the sea chest obtained from a simulated calculation result. The red line in the flow velocity distribution indicates the circulating flow.

6. Conclusion

For the development and design of MALS, which applies an air lubrication method that reduces frictional drag by mixing air bubbles of millimeter order into the flow around the hull, the utilization of simulation technology is essential. A CFD-based prediction technology for air bubble distribution around a hull and a prediction technology for the frictional drag reduction effect using MHI's own frictional drag reduction model are key technologies for the estimation of the energy-saving effect of MALS. The estimation results are roughly consistent with the results of actual ship tests, indicating that these simulation technologies are sufficiently applicable to design. A prediction technology for the pressure fluctuation of a propeller that rotates in the bubbly flow has the potential of turning the disadvantageous risk of increasing propeller pressure fluctuation in a ship equipped with MALS into the advantage of reducing the pressure fluctuation of a propeller. This is assuming that a technology for controlling void fraction distribution at the location of the propeller is developed in the future. A technology for gas-liquid separation in a sea chest can be utilized for the examination of the shapes and internal structures of a sea chest that are effective for the prevention of air bubble intrusion into a cooling water pump. MHI will continue to utilize data from actual ships equipped with MALS in simulation technologies, aiming at the enhancement of simulation accuracy, further improvement in the performance of MALS, and the expansion of ship types to which MALS is applicable.

References

1. Mizokami, S. et al., Experimental Study of Air Lubrication Method and Verification of Effects on Actual Hull by Means of Sea Trial, Mitsubishi Heavy Industries Technical Review Vol. 47 No. 3 (2010) pp.41-47
2. Mizokami, S. et al., Implementation of Ship Energy-Saving Operations with Mitsubishi Air Lubrication System, Mitsubishi Heavy Industries Technical Review Vol. 50 No. 2 (2013) pp.44-49
3. Kawakita, C., Estimation of Frictional Drag Reduction Effect for the Ship with Air Lubrication System, Conference Proceedings the Japan Society of Naval Architects and Ocean Engineers (19) 2014A-JK-2
4. Kawakita, C., Study on the increase or decrease of pressure fluctuation of marine propeller running in bubbly flow, Conference Proceedings the Japan Society of Naval Architects and Ocean Engineers (19) 2014A-GS7-6